Intense red upconversion luminescence from Tm^{3+}/Yb^{3+} codoped transparent glass ceramic

Wei Xu,[1] Jianmin Chen,[1] Peng Wang,[1] Zhiguo Zhang,[1,2,4] and Wenwu Cao[1,3,5]

[1]*Condensed Matter Science and Technology Institute, Harbin Institute of Technology, Harbin 150001, China*

[2]*Laboratory of Sono- and Photo-theranostic Technologies, Harbin Institute of Technology, Harbin 150001, China*

[3]*Materials Research Institute, The Pennsylvania State University, Pennsylvania 16802, USA*

[4]*e-mail: zhangzhiguo@hit.edu.cn*

[5]*e-mail: dzk@psu.edu*

Received November 11, 2011; revised November 27, 2011; accepted November 27, 2011; posted November 29, 2011 (Doc. ID 158093); published January 12, 2012

Tm^{3+}/Yb^{3+} codoped transparent glass ceramic containing β-PbF_2 nanocrystals was successfully prepared. After thermal treatment, emissions from the $^1G_4$ state of Tm^{3+} excited by 980 nm laser were greatly quenched by cross relaxation and the 700 nm luminescence from Tm^{3+}:$^3F_{2,3} \rightarrow {}^3H_6$ transition was strongly enhanced. A nearly monochromatic red luminescence band was observed. Based on the luminescence decay curves and Judd–Ofelt analysis, the strengthened cross relaxation played an important role in such phenomenon.

OCIS codes: 160.5690, 300.6550.

Upconversion (UC) emissions of trivalent rare-earth (RE) ions have attracted a lot of attention for their wide applications in solid-state lasers, sensors, and high-density memories [1–3], and so on. Among the RE ions, Tm^{3+} has been extensively investigated for producing UV to IR luminescence [4,5]. Because of the large absorption cross section around 980 nm, Tm^{3+} is usually used as the sensitizer. In most previous investigations, the red UC emission (700 nm) from Tm^{3+}:$^3F_{2,3} \rightarrow {}^3H_6$ is often neglected or cannot be detected due to the low luminescence intensity, but the existence of this emission is theoretically known. Therefore, it is of technological importance and scientific interest to explore this wavelength emission.

The energy level diagram of Tm^{3+} and some of the possible cross-relaxation (CR) channels for the $^1G_4$ state are depicted in Fig. 1. According to the Dexter theory [6], the CR probability is proportional to R^{-6}, where R is the distance between RE ions. As a result, such abundant CR channels make the emissions from the $^1G_4$ state very sensitive to the change of the distance between Tm^{3+} ions. Among these CR channels, CR1:$^1G_4 + {}^3H_6 \rightarrow {}^3F_{2,3} + {}^3F_4$ can easily take place due to the small energy mismatch

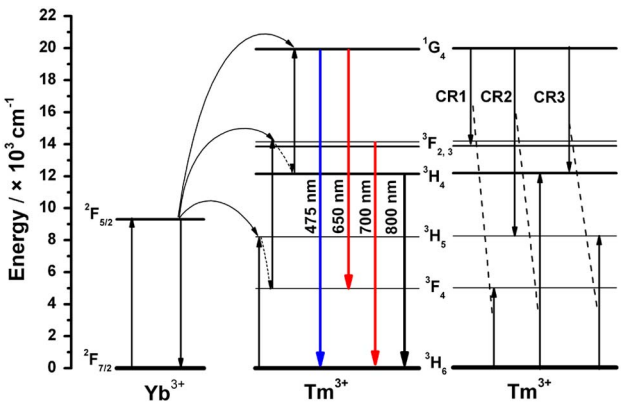

Fig. 1. (Color online) Energy level diagram of Tm^{3+} and Yb^{3+} and the possible cross-relaxation channels, as well as processes generating blue, red, and near-IR UC emissions.

(about 493 cm^{-1} determined by the absorption spectra in our experiment). Additionally, CR1 can also populate the $^3F_{2,3}$ levels and further enhance 700 nm UC luminescence. Therefore, it is possible to obtain a bright and monochromatic 700 nm red emission band by the enhancement of CR processes through decreasing the distance between Tm^{3+} ions.

We choose the oxyfluoride glass ceramic as the host material in our investigations. Through thermal treatment of the precursor glass, the RE ions can be incorporated into the fluoride nanocrystals, which can effectively reduce the distance between the doping ions. Based on this mechanism, the chemical composition and the sample preparation routine were designed to produce 700 nm UC luminescence.

Transparent glass ceramic was obtained through thermal treatment of the precursor glass. The samples were doped with Tm^{3+} and Yb^{3+} with relatively high concentration. Under 980 nm laser excitation, our sample yields an intense and nearly monochromatic red luminescence band centering at 700 nm. The mechanisms leading to such interesting phenomenon are investigated by analysis based on the luminescence decay curves and Judd–Ofelt (J-O) theory.

The glass ceramic is prepared with the following starting composition ratios (in mol. %): $50SiO_2$–$50PbF_2$–$0.5Tm_2O_3$–$5Yb_2O_3$. The fully mixed chemicals are melted in a covered alumina crucible at 1000 °C for 1 h in a SiC-resistance electric furnace in air. Then, the melt is casted into a preheated stainless steel mold and naturally cooled down to room temperature to form the precursor glass. The precursor glass is heated to 470 °C with a heating rate of 10 K/min, and then held for 8 h to form transparent glass ceramic through crystallization. These treatment conditions were set empirically. The resulting samples are cut and polished into the size of 10 mm × 5 mm × 2 mm for optical measurements. X-ray diffraction (XRD) patterns were acquired using a Rigaku $D/_{max-\gamma}B$ diffractometer with Cu $K\alpha$ radiation ($\lambda = 0.15418$ nm). The UC luminescence spectra were recorded by a Zolix-SBP300 grating spectrometer equipped with a

CR131 photomultiplier tube. A 980 nm diode laser is used as the pump source. The luminescence decay curves were recorded by a Tektronix DPO 4140 oscilloscope and the absorption spectra were measured with a fluorospectrophotometer. All measurements were carried out in ambient pressure and at room temperature.

The XRD patterns of the glass and the glass ceramic are shown in Fig. 2. There are only two humps in the XRD curve for the glass, indicating its amorphous structure. However, after thermal treatment, intense diffraction peaks attributed to β-PbF_2 nanocrystals [7] emerged in the XRD patterns, reflecting the crystallization during thermal treatment. The nanocrystal size is estimated to be about 20 nm in diameter by the Debye–Scherrer formula.

The absorption spectra of samples are shown in Fig. 3. The marked absorption peaks correspond to the transitions from the ground state $^3H_6$ to the excited states of Tm^{3+} and the transition from $^2F_{7/2}$ to $^2F_{5/2}$ of Yb^{3+}. The inset of Fig. 3 is the enlarged absorption part between 660 and 820 nm. It can be seen that, after crystallization, the $^3H_6 \rightarrow {}^3F_{2,3}$ transition becomes sharper and the absorption maximum for the $^3H_6 \rightarrow {}^3H_4$ transition changes from 791 to 776 nm. These observations indicate that most RE ions have successfully entered into the β-PbF_2 nanocrystals after thermal treatment [8]. Based on the data deduced from the absorption spectra, J-O parameters $\Omega_t (t = 2, 4, 6)$ were determined by the J-O theory [9,10]. Generally speaking, the intensity parameter Ω_2 is sensitive to the local symmetry environment around RE ions, and it decreases from oxide to fluoride [11]. The calculated value of Ω_2 (about 2.76×10^{-20} cm^2) in the glass ceramic is smaller than that of the glass (about 3.40×10^{-20} cm^2). These results further verify the incorporation of Tm^{3+} and Yb^{3+} ions into the β-PbF_2 nanocrystals.

Figure 4 shows the UC emission spectra of both the glass and the glass ceramic excited by a 980 nm laser with its pump power at 350 mW. Emission bands of the glass, which are attributed to the $^1G_4 \rightarrow {}^3H_6$ (475 nm), $^1G_4 \rightarrow {}^3F_4$ (650 nm), $^3F_{2,3} \rightarrow {}^3H_6$ (700 nm), and $^3H_4 \rightarrow {}^3H_6$ (800 nm) transitions of Tm^{3+}, are observed. In the visible UC spectrum of the glass, blue emission is dominant, as shown by the inset of Fig. 4(a). For the glass ceramic, the blue and red (650 nm) emissions are greatly quenched so that they become negligible compared to the 700 nm luminescence. On the contrary, the red UC emission from the $^3F_{2,3} \rightarrow {}^3H_6$ transition is enhanced by a factor of 3.5 compared to that of the glass, and the 800 nm near-IR (NIR) emission is also greatly increased. Bright red luminescence can be clearly seen by naked eyes, as presented by the inset of Fig. 4(b). Because of the great luminescence quenching of the $^1G_4$ state, the intensity of 475 and 650 nm emissions keeps much smaller values compared with that of 700 nm luminescence, although the intensity ratio between them can be adjusted by changing the pump power. Therefore, intense 700 nm emission, a quasi-monochromatic red luminescence band in the visible range, has been obtained in the glass ceramic under a 980 nm laser excitation.

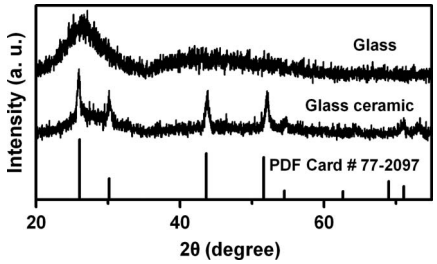

Fig. 2. XRD patterns of the precursor glass and glass ceramic.

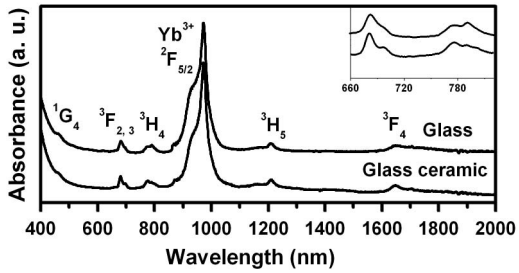

Fig. 3. Absorption spectra for the glass and the glass ceramic; the inset shows the enlarged part between 660 and 820 nm.

The weakening of emissions from the Tm^{3+}:$^1G_4$ state when the glass becomes glass ceramic probably originate from the enhanced cross relaxations by crystallization. To confirm this mechanism, the cross-relaxation rate was calculated by the following equation:

$$1/\tau = 1/\tau_{\text{rad}} + W_{\text{ph}} + W_{\text{cr}}, \tag{1}$$

where τ is the luminescence decay time; τ_{rad} is the radiation lifetime, W_{ph} is the phonon-assisted nonradiation relaxation rate, W_{cr} is the cross-relaxation rate. The luminescence decay curves for the Tm^{3+}:$^1G_4$ state in the glass and glass ceramic are shown in Fig. 5(a). The values of τ are 150 and 45 μs for the $^1G_4$ state in the glass and in the glass ceramic, respectively. W_{ph} can be ignored due to the large energy gap from $^1G_4$ to the next level. The parameter τ_{rad} can be calculated based on the J-O theory [12]:

$$\tau_{\text{rad}} = \frac{1}{A_{\text{ed}} + A_{\text{md}}}, \tag{2}$$

$$A_{\text{ed}} = \frac{64\pi^4 e^2}{3h(2J+1)\lambda^3} \times \frac{n(n^2+2)^2}{9} \sum_{t=2,4,6} \Omega_t |\langle \gamma J \| U^{(t)} \| \gamma' J' \rangle|^2, \tag{3}$$

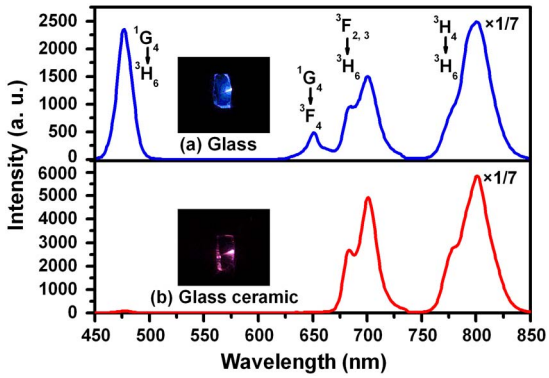

Fig. 4. (Color online) Upconversion emission spectra of (a) the precursor glass and (b) the glass ceramic under 980 nm laser excitation; the insets of (a) and (b) show photographs of luminescence from the glass and the glass ceramic.

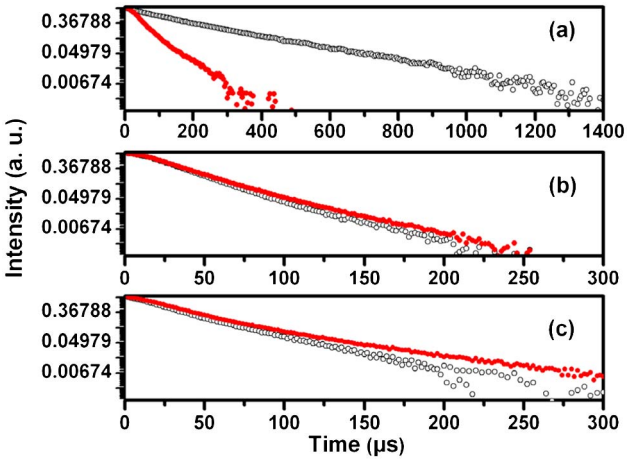

Fig. 5. (Color online) Luminescence decay curves for the (a) $^1G_4$, (b) $^2F_{2,3}$, and (c) $^3H_4$ states in the precursor glass (open black symbols) and glass ceramic (solid red symbols).

$$A_{\mathrm{md}} = \frac{4\pi^2 e^2 h n^3}{3m^2 c^2 (2J+1)\lambda^3} |\langle \gamma J \| L + 2S \| \gamma' J' \rangle|^2. \quad (4)$$

The meaning of the parameters in Eqs. (2), (3), and (4) can be consulted in [12]. Finally, the calculated W_{cr} for the $^1G_4$ state in the glass ceramic is about 19.999×10^3 s^{-1}, which is about 4.7 times the value for the glass (4.286×10^3 s^{-1}). This result confirms the enhancement of CR processes after crystallization. Furthermore, it is worth pointing out that the measured luminescence lifetime for $^3F_{2,3}$ states is hardly changed (from 23 to 24 μs) after thermal treatment, as shown in Fig. 5(b). This means that the enhancement of 700 nm UC luminescence is mainly due to the increased population of the $^3F_{2,3}$ states, which is attributed to several reasons. First, the increased CR1:$^1G_4 + {}^3H_6 \rightarrow {}^3F_{2,3} + {}^3F_4$ plays an important role in weakening emissions from the $^1G_4$ state and enhancing the population in the $^3F_{2,3}$ states. Second, the much-enhanced energy transfer (ET) from Yb^{3+} to Tm^{3+} in the glass ceramic also contributes. After crystallization, the distance between Tm^{3+} and Yb^{3+} is reduced because of the incorporation of RE ions into the fluoride nanocrystals. Based on Dexter theory [13], a shorter distance between sensitizer and acceptor is of benefit for the enhancement of ET efficiency. As a result, the efficiency of the excitation state absorption process $^3F_4 \rightarrow {}^3F_{2,3}$ via ET from Yb^{3+} to Tm^{3+} is increased, and contributes to the population in the $^3F_{2,3}$ states. Third, the enhanced population of the $^3F_4$ state after crystallization also contributes. Through the CR processes (CR1, CR2, CR3, and $^3H_4 + {}^3H_6 \rightarrow {}^3F_4 + {}^3F_4$), more Tm^{3+} ions can be populated in the $^3F_4$ state. Some of these ions come back to the ground state by radiative or nonradiative transitions, and some are being pumped to the $^3F_{2,3}$ states via ET from Yb^{3+} to Tm^{3+}, which finally increases the population of $^3F_{2,3}$ states. Meanwhile, through the Tm^{3+}:$^3H_4$ state luminescence decay curves in the precursor glass and glass ceramic shown in Fig. 5(c) (changing from 44 to 48 μs), it is clearly seen that these CR processes also give important contribution to the enhancement of 800 nm NIR emission.

In conclusion, we have demonstrated that intense and nearly monochromatic red UC luminescence band centering at 700 nm can be produced via crystallization of Tm^{3+}/Yb^{3+} codoped SiO_2-PbF_2 oxyfluoride glass. The UC emissions from the Tm^{3+}:$^1G_4$ state are greatly quenched by cross relaxation, which is confirmed by theoretical analysis based on the luminescence decay curves and J-O theory. The increased CR processes combine with higher efficiency of ET from Yb^{3+} to Tm^{3+}, which are induced by the RE incorporation into the β-PbF_2 nanocrystals, greatly enhance the population of $^3F_{2,3}$ states, and, consequently, increase 700 nm red UC luminescence. This interesting characteristic of Tm^{3+}/Yb^{3+} codoped β-PbF_2 transparent glass ceramic may be used to design devices to meet specific color demands, such as in the fields of optics and solid-state lasers.

References

1. E. Heumann, S. Bär, H. Kretschmann, and G. Huber, Opt. Lett. **27**, 1699 (2002).
2. E. Heumann, S. Bär, K. Rademaker, G. Huber, S. Butterworth, A. Diening, and W. Seelert, Appl. Phys. Lett. **88**, 061108 (2006).
3. F. Lahoz, S. E. Hernández, N. E. Capuj, and D. Navarro-Urrios, Appl. Phys. Lett. **90**, 201117 (2007).
4. R. Balda, L. M. Lacha, J. Fernández, M. A. Arriandiaga, J. M. Fernández-Navarro, and D. Muñoz-Martin, Opt. Express **16**, 11836 (2008).
5. D. Q. Chen, Y. S. Wang, Y. L. Yu, F. Liu, and P. Huang, Opt. Lett. **32**, 3068 (2007).
6. D. L. Dexter, J. Chem. Phys. **22**, 1063 (1954).
7. J. Qiu, R. Kanno, Y. Kawamoto, Y. Bando, and K. Kurashima, J. Mater. Sci. Lett. **17**, 653 (1998).
8. F. Lahoz, J. M. Almenara, U. R. Rodríguez-Mendoza, I. R. Matín, and V. Lavín, J. Appl. Phys. **99**, 053103 (2006).
9. B. R. Judd, Phys. Rev. **127**, 750 (1962).
10. G. S. Ofelt, J. Chem. Phys. **37**, 511 (1962).
11. M. Bettinelli, A. Speghini, M. Ferrari, and M. Montagna, J. Non-Cryst. Solids **201**, 211 (1996).
12. T. Y. Ivanova, A. A. Man'shina, A. V. Kurochkin, Y. S. Tver'yanovich, and V. B. Smirnov, J. Non-Cryst. Solids **298**, 7 (2002).
13. D. L. Dexter, J. Chem. Phys. **21**, 836 (1953).